Analysis of Bed Agglomeration During Gasification of Wheat Straw in a Bubbling Fluidised Bed Gasifier Using Mullite as Bed Material

Seán T. Mac an Bhaird[a], Eilín Walsh[a*], Phil Hemmingway[a], Amado L. Maglinao[b], Sergio C. Capareda[b], Kevin P. McDonnell[c]

[a] School of Biosystems Engineering, University College Dublin, Belfield, Dublin 4, Ireland

[b] Department of Biological and Agricultural Engineering, Texas A&M University, College Station, Texas, USA

[c] School of Agriculture and Food Science, University College Dublin, Belfield, Dublin 4, Ireland

Abstract

The quantity and composition of the ash content of straw poses technical challenges to its thermal conversion and have been widely reported to cause severe ash sintering and bed agglomeration during fluidised bed gasification. Literature indicates that a combination of reactor design and bed material measures is required to avoid defluidisation at temperatures above 800 °C. Using scanning electron microscopy and energy dispersive X-ray spectroscopy this study investigated the initial agglomeration of a mullite bed during the gasification of wheat straw in a small scale, air blown bubbling fluidised bed. The results show that the temperatures along the height of the bed converge prior to any marked drop in pressure or heating of the lower freeboard. This convergence was seen to occur at temperatures close to 750 °C in repeated gasification experiments. Energy dispersive X-ray spectroscopy indicates coating-induced agglomeration caused by the reaction of alkali metals with silica. Scanning electron microscopy under high magnification revealed a layered structure to the agglomerates, where ash particles are subsumed into a fused material. This suggests the formation of agglomerates by the three step agglomeration process postulated by other authors. Analysis of indices used to predict agglomeration on the basis of a fuel's ash content and composition indicate that the Alkali Index is the most accurate, successfully predicting agglomeration for 7 of the 9 fuels where agglomeration

* Corresponding author: email eilin.walsh@ucd.ie, tel. +353 1 716 7458, fax + 353 1 716 7415

was observed.

Keywords: Bubbling Fluidised Bed, Gasification, Wheat Straw, Mullite, Bed Agglomeration, Predictive Indices

1. Introduction

The gasification of wood has been successfully demonstrated in numerous conversion plants throughout Europe. In comparison, the experience with other biomass fuels is limited as the performance of a gasifier is affected by biomass type [1]. Straw is a prime example where a lack of engineering expertise relating to its gasification characteristics has been identified [1]. The technical reliability of straw gasification systems has been classified as low, outranked marginally by sludge and significantly by woody biomass which has the highest reliability. These reliability issues are associated with severe problems of ash sintering and bed agglomeration [2] which are influenced by the composition of the fuel . Ash-related problems have been identified as the main obstacle to the realisation of viable and economic applications of biomass gasification [3]. Bed agglomeration is often a precursor to the unscheduled shut-down of fluidised bed gasifiers [4] and is the foremost ash-related problem affecting the performance of fluidised beds. The alkali content of the biomass is seen as the main contributor [5].

The two major pathways to agglomeration are *melt-induced* and *coating-induced* agglomeration [6]. The less common melt-induced process relates to particles adhering together by a molten phase whose chemical structure is similar to that of the fuel ash [7]. This mechanism is associated predominantly with fuels with elevated alkali, sulphur, and chlorine contents which form low melting point eutectics [6]. The more typical coating-induced mechanism involves a sticky layer forming on the surface of particles and fusing individual particles together [6]. The sintering of these coatings initiates agglomeration and where ash melting does not occur, full agglomeration proceeds [7, 8]. This process is associated with the reaction of alkalis with silica or sulphur. Reactions between alkali and alkali metals (mainly potassium) and the bed material of silica sand have been reported as initiating this coating process [8] but there have been conflicting views [6].

A fuel's tendency to cause agglomeration is mainly dependent on temperature and the ash composition and content of the fuel. Temperature is known to have a significant impact on

the agglomeration process and has been highlighted as the most important parameter in fluidised bed gasifiers, with higher temperatures increasing agglomeration tendencies [3]. Temperature uniformity is important in combating agglomeration. Fluidised bed reactors, with their relatively low operating temperatures and isothermal operating conditions [9], are therefore attractive for use with fuels which pose ash-related problems. Slagging is generally associated with fuels with ash contents which exceed 5-6% and severe slagging may prevail when ash contents are greater than 12%.

Compared to the influence of temperature, the effects of ash composition are less well understood. Generalised estimates have been established and utilised to develop indices to predict agglomeration tendencies on the basis of a fuel's ash composition and content. The reliability of such indices has, however, been questioned [7] as they do not take account of the influence of the bed material on the process. For example, the ash fusion temperature is seen as not predicting agglomeration in all cases and although it is widely employed, the standard American Society for Testing and Materials (ASTM) ash fusion test [10] is inadequate for predicting ash-related problems for biomass and energy crops [11]. With this in mind such indices should be used only as a general guide to ash behaviour.

Widely-adopted predictive indices include the Alkali Index, the Bed Agglomeration Index, and the Base to Acid Ratio. The Alkali Index is based on the ratio of K_2O and Na_2O to the higher heating value (HHV) and is calculated as follows:

$$\text{Alkali Index (kgGJ}^{-1}) = (1*10^6/\text{HHV}_{\text{dry basis}})* \text{ wt\% } (K_2O + Na_2O)$$

where HHV = the higher heating value of the fuel (kJkg^{-1}); and

wt% = the weight percentage of the ash components in the fuel.

Fuels with Alkali Index values which exceed 0.17 kgGJ^{-1} are deemed to be problematic, while fouling and slagging will most likely occur with ratios in excess of 0.34 kgGJ^{-1}. Where the HHV of the fuel is unavailable for the calculation of the Alkali Index, the following correlation derived by Parikh et al. [12] can be utilised:

$$\text{HHV (MJkg}^{-1}) = -3.0368 + (0.2218*\text{VM}) + (0.2601*\text{FC})$$

where VM = volatile matter content; and

FC = fixed carbon content, each reported on a dry basis.

Agglomeration is also associated with Bed Agglomeration Index (BAI) values of lower than 0.15 [13]. The BAI is calculated as:

$$BAI = \%(FE_2O_3) / \%(K_2O + Na_2O)$$

Another index widely used to predict the ash behaviour of a fuel is the Base to Acid Ratio ($R_{b/a}$). It was developed for fossil fuels with low phosphorous quantities and in its original form does not take account of the increased fouling tendencies associated with phosphorous in the form of P_2O_5. As the P_2O_5 content of biomass fuels is relatively high the calculation has been modified as follows to take P_2O_5 into account Kupka et al. [14]:

$$R_{b/a} = \%(Fe_2O_3 + CaO + MgO + K_2O + Na_2O + P_2O_5) / \%(SiO_2 + TiO_2 + Al_2O_3)$$

The greater the value of the $R_{b/a}$ the higher the likelihood of ash-related problems. A low deposition tendency has been associated with $R_{b/a}$ values less than 0.5; a medium deposition tendency with $R_{b/a}$ values between 0.5 and 1; and a high deposition tendency with $R_{b/a}$ values greater than 1 [13].

The focus of this research work is the agglomeration process during the gasification of wheat straw in a small scale, air blown bubbling fluidised bed gasifier. The agglomerates formed were examined in terms of their quantity, structure, and composition with the aid of scanning electron microscopy (SEM) and energy dispersive X-ray spectrometry (in literature energy dispersive X-ray spectrometry has been abbreviated to both EDX and EDS. In this text it will be referred to as EDS). The ability to accurately predict agglomeration from the ash content and composition of the fuel through use of the Alkali Index, the Bed Agglomeration Index, and the Base to Acid Ratio was also investigated.

2. Materials and Methods

2.1 Apparatus and Operating Conditions

A bubbling fluidised bed (BFB) gasifier developed by Texas A&M University ([15], United States Patent number 4,848,249) was used to study the gasification characteristics of wheat straw. The gasifier was designed to accommodate cotton gin trash and similar biomass without the need for pre-conditioning [15]. A range of feedstocks in a variety of particle sizes have been successfully gasified to date including poultry litter, wood chips, cotton gin trash, dairy manure, sorghum, and switchgrass [15-17]. The gasification agent utilised in all

studies was air. The design power output of the gasifier was set at approximately 73 kW based on the heating value of the producer gas from the gasification of cotton gin trash.

A natural gas burner is employed to preheat the air to the gasifier to reach operating temperatures. Bubble caps are adopted in place of the previous twin distributor plate arrangement. The fuel is fed into the gasifier via an auger system; an optical counter is used to measure the rotational speed of the auger feeding the fuel directly into the bottom of the bed, close to the distribution plate. This feed configuration minimises segregation of the fuel from the bed which can have a detrimental effect on the performance of a gasifier: segregation of the fuel from the bed is linked to higher levels of tar, reduced carbon conversion efficiency, and potentially increased agglomeration [18]. Fuel segregation is known to occur with straw and it is recommended that the fuel be fed directly into the bed [18].

The producer gas exiting the gasifier passes through two cyclones in series which are constructed from cast refractory material. The first cyclone is designed to reduce the particulate loading to a maximum of 3 gm^{-3} and the second to a maximum of 0.5 gm^{-3}. The maximum pressure drop across the two cyclones is 203 mm of water. Collection bins for the recovered particles are located at the bottom of each cyclone. One K-type thermocouple (Omega CAIN-14U, Omega Engineering Inc., Stamford, CT) is located just below the bed base; three further thermocouples are placed along the height of the bed at 152.4 mm, 254 mm, and 469.4 mm above the bed base. Temperature readings from these thermocouples are referenced as T1 to T4, respectively. A laminar flow element is located between the blower and the gasifier to determine the primary air flow rate to the gasifier. Further pressure readings are taken at the bed base and the upper base of the fluidised bed by differential pressure transmitters (Omega PX274: Omega Engineering Inc., Stamford, CT, and Dwyer Series 677: Northeast Controls Inc., Upper Saddle River, NJ). Pressure and temperature are continuously monitored and logged using an Omega OM-320 data logger (Omega Engineering Inc., Stamford, CT). Three gasification tests were conducted as detailed in Table 1. After each gasification test the gasifier was cooled by stopping the flow of biomass into the reactor while allowing the cooling air to continue to flow through the reactor to maintain fluidisation and to allow the auto-ignition temperature inside the reactor to fall below 500 °C. Once the temperature inside the reactor had fallen below 500

°C the air blower system was shut down.

Table 1: Operating conditions adopted in the three gasification tests studying agglomeration in the small scale bubbling fluidised bed gasifier.

Run	Fuel	Average Equivalence Ratio	Average Bed Temperature (°C)[1]
1	Wheat Straw	0.27	770
2	Wheat Straw	0.23	728
3	Wheat Straw	0.17	654

[1]The bed temperature is taken as the average of the readings from thermocouples T2, T3, and T4

2.2 Feedstock and Bed Material

Wheat straw sourced in Texas, United States of America, was utilised for all experiments. Proximate and ultimate analyses of the fuel were conducted in accordance with Maglinao and Capareda [17]. To allow for ready fuel feeding into the gasifier, a hammer mill was used to reduce the size of the fuel to enhance feeding.

Mullite, an alumina sand which has been used to counteract agglomeration tendencies in fluidised beds [19], was used as bed material. Its adoption has seen the successful gasification of wheat straw in a BFB gasifier of novel dual distributor type design at temperatures greater than 900 °C [19]. The Mulcoa 47 mullite, procured from C-E Minerals (Roswell, GA), was passed through a 425 µm USA standard sieve meeting ASTM E 11 specification and the gasifier was filled to just below the disengagement zone, equal to 40 kg of bed material added to the gasifier; the height of bed materials in the gasifier was 0.500 m. Fresh bed material was used for each run. The particle size distribution of the mullite is shown in Table 2.

Table 2: Particle size distribution of mullite used as bed material (after C-E Minerals [20])

USS Sieve Grade	8 2.36 mm	12 1.70 mm	14 1.40 mm	20 850 μm	30 600 μm	40 425 μm	50 300 μm	70 212 μm	100 150 μm	140 106 μm	200 75 μm	270 53 μm	325 45 μm	PAN*
10x18[1]	0-3	10-25		60-82	0-15									0-5
10x28[1]	0	15-25	45-65	6-16	5-15	0-6								0-2
14x28[1]		0	1 max	30-55	35-45	10-25	5 max							1.5 max
16x30[1,2]			0-3	65-75		4 max								1 max
22S[1,2]			TR	15-25	32-47	27-37	4-10						3 max	TR
35S[1,2]			TR	1-5	21-38	40-54		9-19		2-8				3 max
50S[1,2]				0	1-9	22-37	26-40	12-22	6-16	1-6				3 max
60S[1,2]					0	0-5	30-48	30-44	9-22	2-7				3 max
20x50[1,2]			TR	0-8	20-50		50-72						2 max	TR
25x80[1,2]				0-5	20 min 30 avg		80-93	7-12						3 max
50x100[1]						TR	5-20		70-86	0-15	3 max		1 max	TR
60x200[1]							0	0-11		65-90	5-20	0-6		3 max
200 IC-C [1,2,3]									TR		15-25			75-85
325 IC-C [1,2,3]									TR				5-15	85-95

*PAN designates the percentage of material passing the last reported screen for each size

Grade available in AL_2O_3 content (1) 47% (2) 60% (3) 70%

2.3 Procedures

The tests commenced by fluidising the mullite bed by gradually increasing the volume flow rate of air entering the gasifier until a decrease in total pressure drop followed by its characteristic flattening out was evident. At this point the bed was fully fluidised and bubbling vigorously. Before fuel feeding commenced the temperature of the gasifier was increased by preheating the air with a natural gas burner. The superficial gas velocity was set at 0.27 ms^{-1} and was maintained throughout the experiment.

After fuel feeding had commenced and the gas burner had been turned off, the fuel feed rate was steadily decreased to obtain the desired operating conditions of temperature and equivalence ratio (ER). For the first two tests the target temperature was 700 °C and an average fuel feeding rate of approximately 0.40 kg straw min^{-1} was maintained. For the third test the target temperature was lower to avoid loss of isothermal conditions: the fuel feed was initiated when the target temperature of 620 °C was reached and the fuel was fed at an initial ER of approximately 0.35 before being reduced to 0.15 over a short period of time. Fuel feed rates were gradually altered to an average fuel feeding rate of 0.90 kg straw min^{-1} once conditions stabilised.

The design of the gasifier did not allow for ash to be removed directly from the gasifier chamber for inventory control. During operation the level of char in the collection bins located at the bottom of each cyclone was continuously monitored and emptied when required. The char was transferred to stainless steel containers which were sealed to reduce air exposure and the potential oxidation of the hot char.

Ashing for ultimate analysis was conducted at 550 and 750 °C. Although lower than the typical ashing temperature of between 580 and 600 °C utilised for biomass, the temperature of 550 °C was adopted to minimise the loss of ash components in line with observations by Fernández Llorente and Carrasco García [21] who suggested an ashing temperature of 500 to 550 °C for herbaceous and woody biomasses. It is also in line with the ashing temperature recommended for straw by the International Energy Agency [22]. The higher temperature of 750 °C corresponds to measurements in accordance with ASTM standard E 1755-01 and was used for all predictive indices calculations in this study.

Following each gasification test and when the gasifier had cooled, bed material was removed using a vacuum and a wire brush to dislodge any material that had adhered to the walls of the reactor. This material was captured in an expandable device comprising of a circular layer of plastic mounted on an arm which could be lowered into the reactor, expanded to cover its entire cross section and capture the material that had been removed from the walls, then collapsed and withdrawn from the reactor. The material removed from the reactor was passed through a 1.7 mm USA standard sieve meeting ASTM E 11 specification to segregate agglomerates from the bed material for analysis.

Agglomerates from each distinct group were examined using SEM and EDS analyses. SEM samples were prepared by first cutting the bulk sample into halves using a razor blade to obtain both top-view and cross-sectional samples. The samples were subsequently placed on an aluminium mount before being coated with a thin conductive film. Measurements were performed on an FEI Quanta 600 (FEI, Hillsboro, OR) field emission scanning electron microscope (FESEM) equipped with a Schottky field emission gun. A conventional Everhart-Thornley detector and Oxford energy dispersive X-ray spectroscopy system attached to the FESEM were used for imaging and elemental analysis. When an area of interest was discovered an image was acquired with 10 to 40 seconds of integration time. EDS spectra were collected from a spot or local region of an area at a 20 kV accelerating voltage with a stationary electron probe. Each spectrum was analysed with INCA microanalysis suite (Oxford Instruments, Austin, TX) to identify component elements.

3. Results and Discussion

3.1 Feedstock

The proximate and ultimate analyses of the wheat straw utilised in the gasification experiments are reported in Table 3. The results are compared to the composition of Irish wheat straw as reported by Caslin and Finnan [23]: it is evident that with the exception of ash content the straws are very similar. The ash content, at just under 11 wt% on a dry basis, is higher than that of woody biomass for which ash contents as low as 2.5% have been reported [24]. Figure 1 compares the ash content observed in this work to those reported for wheat straws in other experiments.

Table 3: Ultimate and proximate analyses of the wheat straw used in this study and that reported for Irish-sourced wheat straw (after Caslin and Finnan [23]).

	This study	Caslin and Finnan [23]
Moisture Content (wt% as received)	8.02	15
Higher Heating Value ($MJkg^{-1}$)	17.52	14.4
Volatile Content (wt% on a dry basis)	81.03 ± 0.27	-
C (wt% on a dry basis)	43.51	45.6
Fixed C (by difference; wt% on a dry basis)	8.21 ±0.28	-
H (wt% on a dry basis)	5.43	5.8
N (wt% on a dry basis)	0.58	0.48
O (wt% on a dry basis)	39.13	42.4
S (wt% on a dry basis)	0.12	0.08
Ash (wt% on a dry basis)	10.76 ± 0.28	6.71

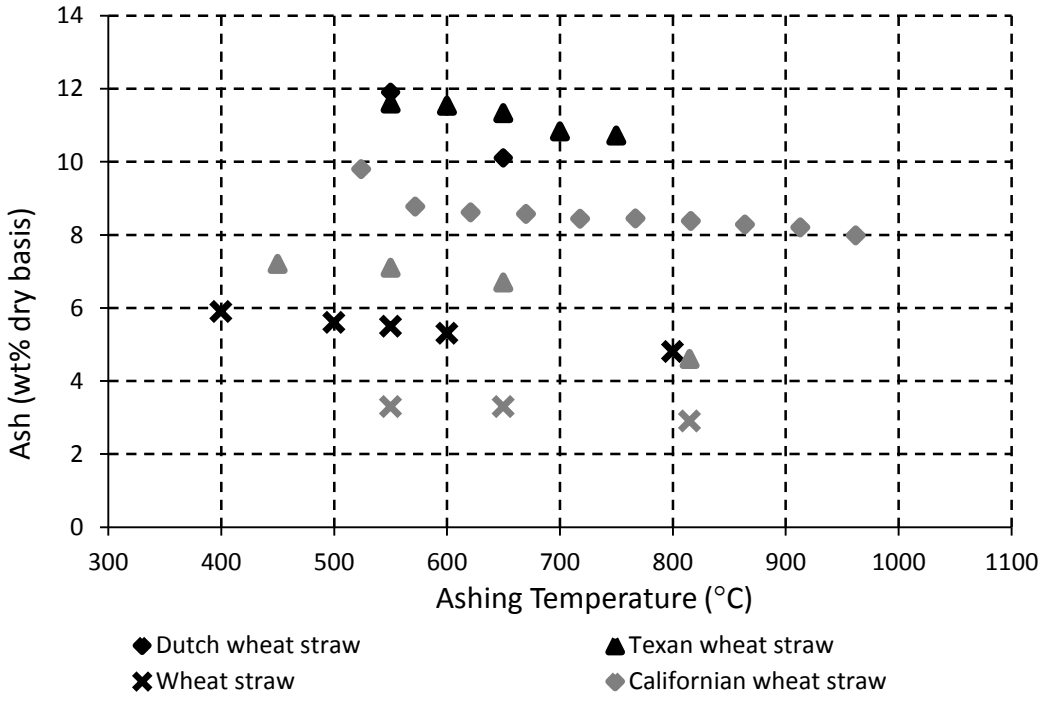

Figure 1: Ash content of wheat straw as determined at different ashing temperatures. Dutch wheat straw [7]; Texan wheat straw (this study); Wheat straw (origin unspecified [21]); Californian wheat straw [25]; Unweathered Danish straw [7]; Weathered Danish wheat straw [7].

3.2 Ash analysis

Results of the ash elemental analyses at both 550 and 750 °C are reported in Table 4.

The main components of the straw were observed to be silicon, potassium, and calcium as was reported by Olanders and Steenari [24]. The higher ashing temperature of 750 °C led to a reduction in SO_3, K_2O, and P_2O_5. The largest change in concentration

Table 4: Ash analysis of the wheat straw used in this study at both 550 and 750 °C (dry basis).

	Elemental composition (wt%)										
Temp. (°C)	Al_2O_3	CaO	Fe_2O_3	K_2O	MgO	MnO	Na_2O	P_2O_5	SiO_2	TiO_2	SO_3
550	0.40	3.55	0.49	21.23	1.32	0.03	0.13	2.99	64.17	0.03	2.57
750	0.42	3.59	0.50	20.17	1.36	0.03	0.13	2.91	64.88	0.03	2.39

was observed for SO_3 which reduced by 7%. The concentrations of K_2O and Al_2O_3 reduced by 5% at the higher temperature. As was observed in other studies, for the temperatures investigated in this study a strong linear inverse correlation between temperature and ash quantity was observed (Figure 1):

$$\text{Ash (wt\% dry basis)} = -0.0049*X + 14.401,\ R^2 = 0.9241$$

where X = ashing temperature (°C)

The ultimate analysis of the wheat straw utilised in this study showed high levels of silica and potassium and low levels of calcium. This is in comparison to the reported concentrations of these elements in woody biomass ash (SiO_2: min. 1.86%, mean 22.22%; K_2O: min. 2.19%, mean 10.75%; and CaO: min. 5.79%, mean 43.03%, Vassilev et al. [26]). The ash content of herbaceous and agricultural straws has been characterised in terms of the relevant mass concentrations of its elements as SiO_2 > K_2O > CaO > MgO > P_2O_5 > Al_2O_3 [26]. The composition of the ash generated in this experimental work follows this pattern with the exception of P_2O_5 and MgO, which are reversed and is the order reported for herbaceous and agricultural biomass and herbaceous and agricultural grass [26].

Table 5 provides a comparison of the indicators used to predict bed agglomeration during gasification in BFBs similar to that used in this study. It can be seen that the ash content of the fuel, Alkali Index and Base to Acid Ratio of the wheat straw fuel indicate that ash-related problems are likely to occur during its gasification. Although agglomeration during gasification was evident for all fuels presented in Table 5, the calculated indices show a lesser probability of agglomeration occurring than for the wheat straw used in this study. Only one indicator, the Alkali Index, highlighted ash-related problems for the other fuels. The Alkali Index did not highlight likely agglomeration for cane trash which was indicated by the $R_{b/a}$ value for this fuel. At 8 wt%, the ash content of olive fuel lies in the region in which agglomeration is

dependent on the ash composition. With no other index pointing to ash problems, this suggests that the agglomeration observed during its gasification is not predictable from the use of the indices presented in Table 5.

Table 5: Comparison of the predictive indices for wheat straw with those for biomass fuels that caused agglomeration during gasification in bubbling fluidised beds

Fuel	Wheat straw				Sorghum	Cane trash	Olive flesh	Giant reed	Sweet sorghum bagasse	Olive bagasse
Gasification agent	Air[a]	Air[19]	Air[27]	Steam[28]	Air[29]	Air[5]	Air[5]	Air[6]	Air[6]	Air[6]
Bed Material	Mullite	Alumina sand	Silica	Olivine	Quartz & olivine			Quartz	Quartz	Quartz
Reported agglomeration temperature (°C)	-	920	800	-	810	834	880	785	810	830
Ash content (wt% db)	11.57	3.41	3.41	12.7	3.7	8.0	9.9	2.6	3.3	2.6
Alkali index (kg GJ^{-1})	0.33	0.67	0.67	1.32	0.55	0.2	0.96	<0.01	<0.001	<0.001
$R_{b/a}$	0.4599	0.02	0.02	0.05	0.02	0.12	0.21	0.03	0.01	0.28
Bed Aggomeration Index	0.0229	2.12	2.12	0.43	1.97	0.2	1.48	0.85	1.59	2.14

a: This study

3.3 Defluidisation

Defluidisation of silica sand during fluidised bed combustion of biomass can be identified by pronounced and sudden pressure decreases across the bed accompanied by significant temperature increases in the lower freeboard [30]. These characteristics are associated with bed channelling and stratified combustion of biomass above the bed. Such temperature and pressure changes were observed in both Run 1 and Run 2 but were not evident in Run 3 where the gasification temperature was maintained below 700 °C. Below this point the temperatures throughout the fluidised bed tracked one another, with the temperatures decreasing from the bed base upwards. The maximum temperature deviation from the bed base to the upper bed was approximately 7% with an average temperature deviation of less than 3.5%. These relatively isothermal conditions were disturbed in the other gasification runs. The disturbances appear to be triggered by the temperature of the bed reaching approximately 750 °C at its base. As shown in Figures 2 and 3, within a few degrees of 750 °C the temperatures within the bed align (the deviation is no greater than 0.32%); the differences are noted to be minimised at 747 °C and 748 °C in Runs 1 and 2, respectively. Once this temperature had been reached and the temperatures in the bed had aligned, a trend was evident where the temperature differences within the bed (relative to that of the bed base) began to increase. This was followed by the upper bed becoming the hottest part of the bed, indicating stratified combustion of biomass above the bed and poor bed fluidisation. In both Run 1 and Run 2 a pronounced drop in the pressure differential across the bed was not evident until after the upper bed temperature became the hottest (after 2,299 seconds in Run 1 and after 830 seconds in Run 2).

(a)

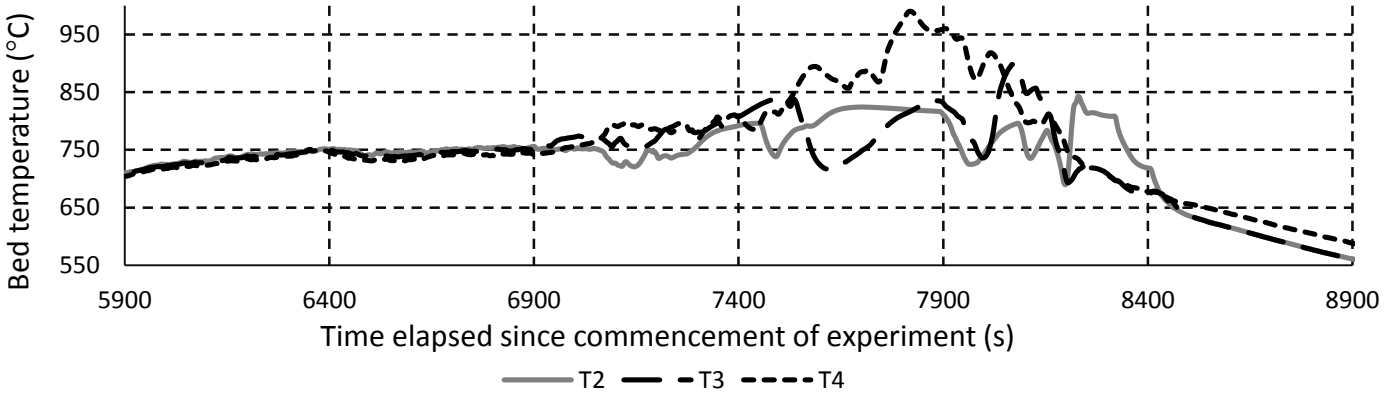

(b)

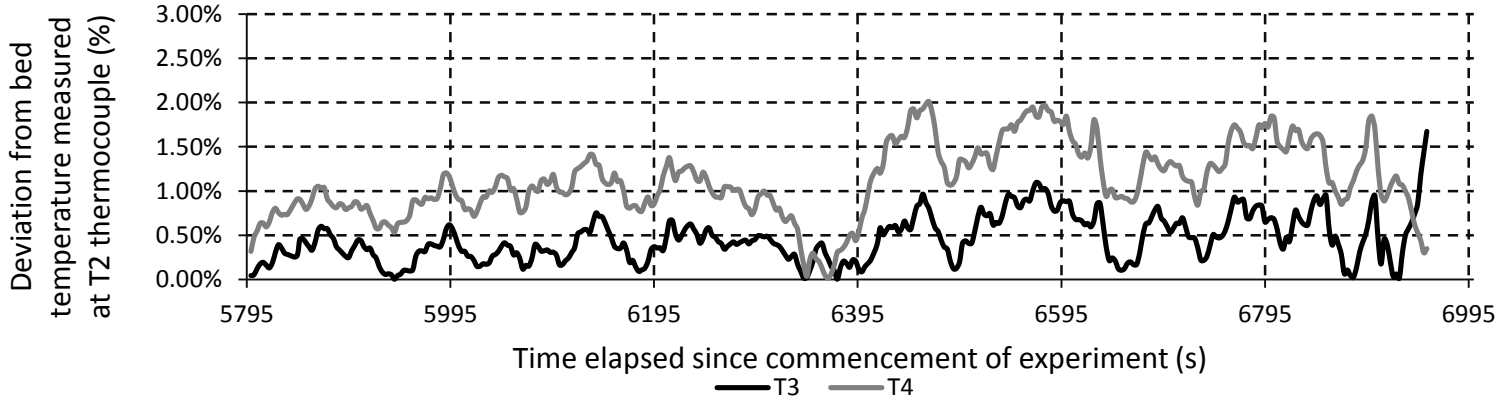

Figure 2: Temperature profile within the small scale bubbling fluidised bed gasifier for Run 1 presented in terms of (a) absolute temperatures and (b) percentage deviation from the temperature measured at the bed base during the gasification of wheat straw with air. T2, T3, and T4 thermocouples positioned 152.4 mm, 254 mm, and 469.4 mm above the bed base, respectively.

(a)

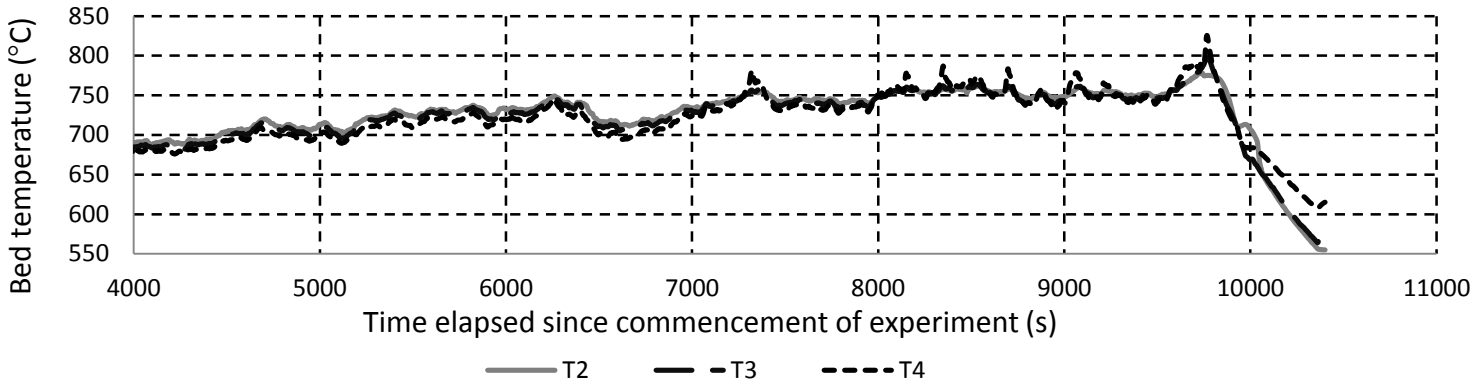

(b)

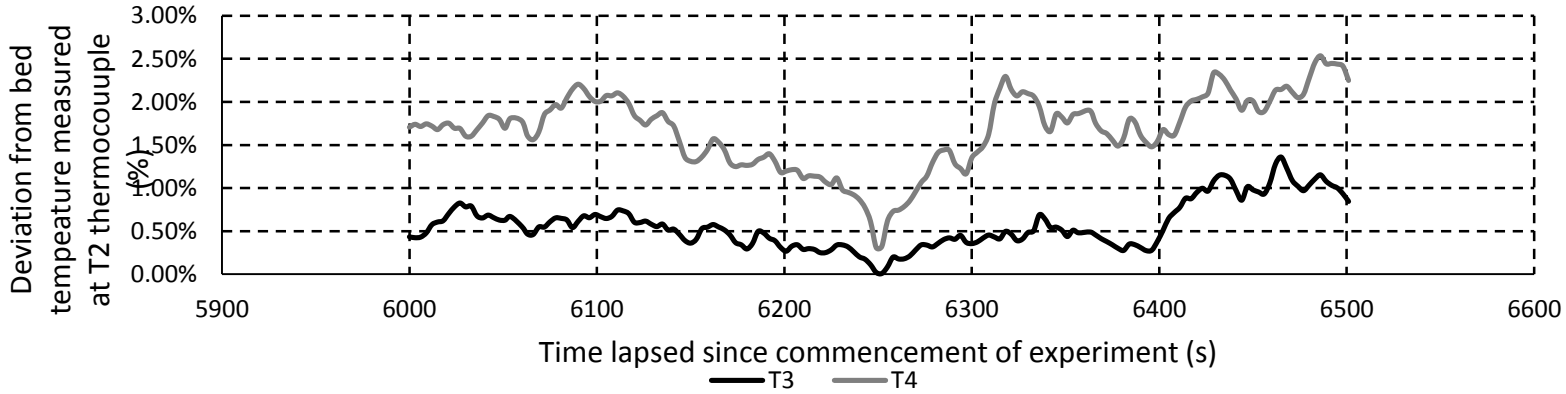

Figure 3: Temperature profile within the small scale bubbling fluidised bed gasifier for Run 2 presented in terms of (a) absolute temperatures and (b) percentage deviation from the temperature measured at the bed base during the gasification of wheat straw with air. T2, T3, and T4 thermocouples positioned 152.4 mm, 254 mm, and 469.4 mm above the bed base, respectively.

The data indicate that temperature alignments within the bed point to the onset of defluidisation at approximately 750 °C. This temperature aligns with that observed by Salour et al [18] who associated the successful gasification of wheat straw with temperatures below 760 °C. It is somewhat lower than the typical agglomeration temperature associated with the gasification of wheat straw (between 800 and 850 °C) reported by Turn et al. [31].

Table 6 compares the observations regarding agglomeration of individual studies reported in the literature to those observed in this study. It can be seen that beyond 800 °C a combination of reactor design and bed material measures were required to avoid defluidisation: gasifiers with simplistic single distributor plate designs and silica sand as bed material were no longer suitable. In contrast, operation without agglomeration has been reported up to 800 °C with the use of an allothermal fluidised bed [32] though no bed material was adopted in this instance. The highest successful gasification temperature without agglomeration of 920 °C was reported by Ergudenler and Ghaly [19]: this was achieved with the use of mullite and a dual distributor type fluidised bed gasifier.

Table 6: Comparison of temperatures of wheat straw conversion in fluidised bed gasifiers and occurrence of bed agglomeration.

Gasifier type	Gasifying agent	Bed Material	Gasification temperature (°C)	Observation
Bubbling fluidised bed (This study)	Air	Mullite	760	Agglomeration
Fluidised bed (dual distributor [19]	Air	Mullite	920	First signs of agglomeration
Fluidised bed (dual distributor) [27]	Air	Silica sand	730 and 740	Agglomeration avoided
Allothermal fluidised bed [28]	Steam	Olivine sand	Up to 710	No problems reported
Allothermal fluidised bed [32]	Air	No bed material	800	No problems reported
Allothermal fluidised bed [7]	Air	Silica sand	810-840	Agglomeration
Novel circulating fluidised bed [33]	Air and steam	Silica sand	825	Agglomeration and sintering
Circulating fluidised bed [34]	Air	Finnish limestone and sand	824	No problems reported. Steam used to control temperature

3.4 Agglomerates

3.4.1 Visual Inspection

Table 7 provides a description of the appearance and mechanical integrity of the particles collected from the bed after the gasifier had cooled. It is evident that the majority of particles consisted of bed material bonded together. The remaining particles appeared to consist of single individual particles which were typically hard and which varied in colour. Particles approaching the colour of terracotta could indicate mild agglomeration [19]. In contrast, the presence of grey particles point to a greater degree of agglomeration while the green colouration evident in particles collected from Run 1 may indicate ash melting [19].

Table 7: A descriptive quantification of the appearance and mechanical integrity of agglomerates formed during the gasification of wheat straw in the bubbling fluidised bed gasifier with air.

Run	Appearance	Quantity (g)	Physical attributes
1	Cluster of grey particles in carbon black material	13.7	Crumble under light to moderate finger pressure
1	Particles attached to globular glassy material	2.1175	Hard
1	Cluster of grey particles with visible sheen	6.811	Break up under light finger pressure
1	Earth tones - terracotta	0.4875	Hard
1	Cluster of grey particles	183.1	Crumble under light to moderate finger pressure
1	Flat grey	0.3252	Crack under moderate finger pressure
1	Lightly coloured	0.3085	Hard
1	Green to yellow in appearance	0.3873	Hard
2	Cluster of grey particles in carbon black material	215.9	Crumble under light to moderate finger pressure
2	Large flat and grey	1.9582	Hard
2	Dark burnt-like colours - terracotta	5.8511	Hard but will crumble under hand pressure
2	Clusters of particles with visible sheen	6.1812	Hard
2	Green-yellow-grey	0.6154	Hard
2	Flate small grey to white	0.4736	Hard
3	Cluster of grey particles in carbon black material	106.7	Crumble with light to moderate finger pressure
3	Terracotta	1.1697	Hard
3	Flat grey	1.3805	Disintegrate under light to moderate finger pressure
3	Metallic (lead-like in appearance)	2.0529	Hard
3	White	0.2569	Hard
3	Lighter larger clusters of grey particles in carbon black material	1.7569	Crumble under moderate finger pressure

3.4.2 SEM and EDS Analysis

Figure 4 shows the morphological analysis of the most abundant agglomerates collected during Run 1. These agglomerates consisted of clusters of grey particles and accounted for approximately 88 wt% of all the agglomerates collected from this test. Visual inspection indicated the absence of carbon black in the bonding structure. SEM analysis revealed a surface consisting of both smooth and rough areas (Figure 4 (a)); particles were partially embedded into the homogenous surface or visible just under the surface. EDS analysis of the rough areas indicated the presence of K, Ca, Al, and Si (Figure 4 (c)). A cross section of the agglomerate showed a porous structure to the binding material (Figure 4 (b)) comprising of K, Ca, Mg, and Si (Figure 4 (d)).

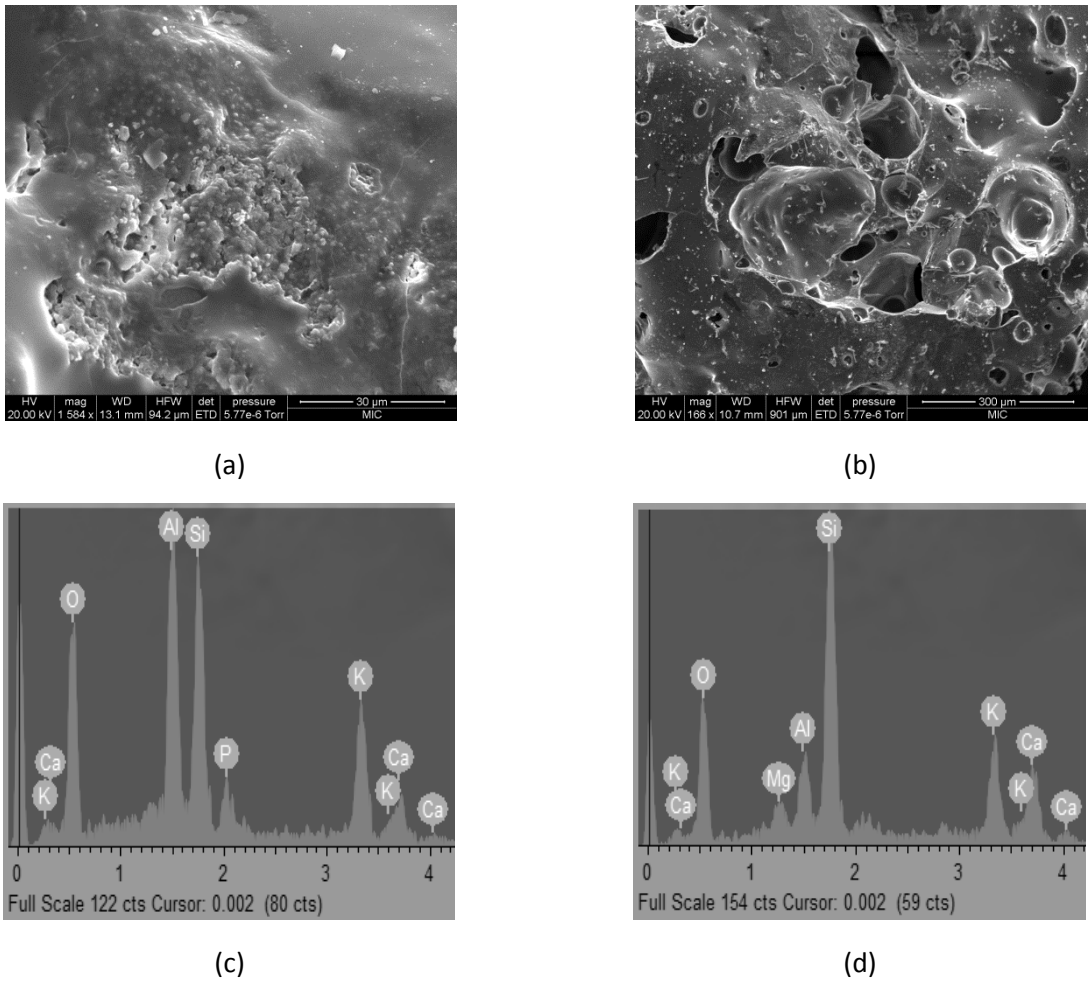

Figure 4: Scanning electron microscopy and energy dispersive X-ray spectrometry analysis of an agglomerate formed in Run 1 where bed material was bonded together in the absence of a distinct black bonding matrix. (a) presents SEM of the surface of the agglomerate; (b) presents SEM of the agglomerate in cross section; (c) presents EDS of the surface of the agglomerate; (d) presents EDS of the cross section of the agglomerate.

In Runs 2 and 3 the vast majority (95 wt%) of agglomerates collected were clusters of bed material bonded by a carbon black matrix; in contrast only 6 wt% of the agglomerates collected in Run 1 showed this structure. The carbon black appearance indicates the presence of unconverted char. An example of such an agglomerate formed in Run 1 is illustrated in Figure 5 which shows the bed material wholly and partially embedded in a porous binding material. Higher magnification of the bed particle, both fused into the porous binding melt and connected to other bed particles via neck-like bonds, revealed its surface to be primarily covered in particles with areas of smooth material: increasing to 16,774 times magnification (Figure 5 (b)) revealed particles encased under the surface of the smooth material which suggests their progressive encasement into the smooth material. Analysis of the porous binding material revealed a smoother surface than that coating the surface of the bed material (Figure 5 (c)). Particles were observed to be adhered to its surface but there was no sign of progressive embedment present.

Examination of a cross section of the porous binding material showed that the smooth and porous nature continues throughout the structure (Figure 5 (d)). It was observed that chambers rather than channels led to the porous-like appearance and that particles were adhered to the walls of these chambers. EDS analysis of the agglomerate indicated the presence of K, Al, and Si at the surface (Figure 5 (e)). Progressive coating of particles as well as porous binding structures was also evident in agglomerates collected from Run 2. EDS analysis identified the presence of Ca in the coating and Cl in the porous binding structure in addition to the elements observed in Run 1. Cl, Ca, K, Fe, and Si were detected in the particles embedded in the porous binding structure. Porous binding structures were also found in the agglomerates formed in Run 3 where K, Ca, and Si were identified by EDS analysis in these structures as well as in the embedded particles.

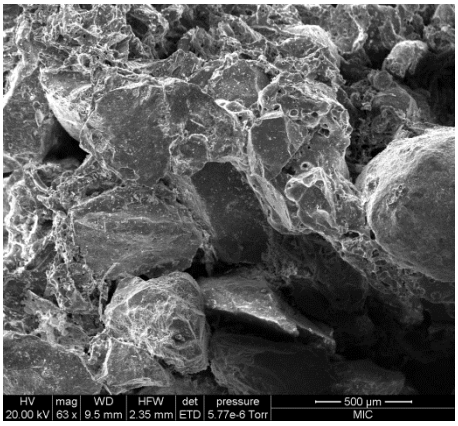

(a)

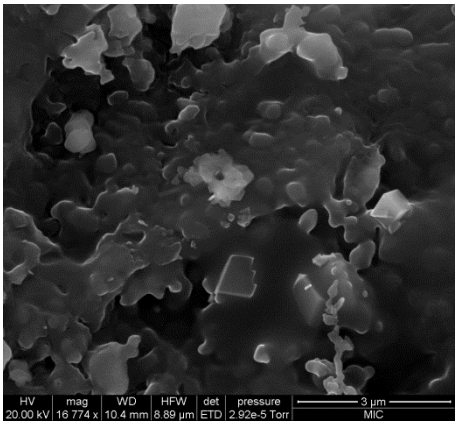

(b)

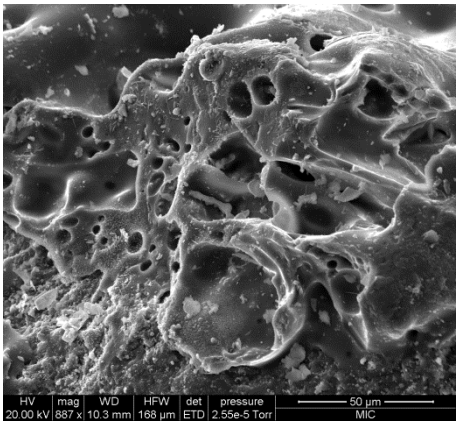

(c)

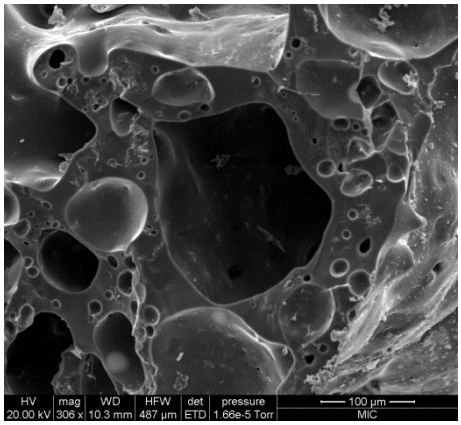

(d)

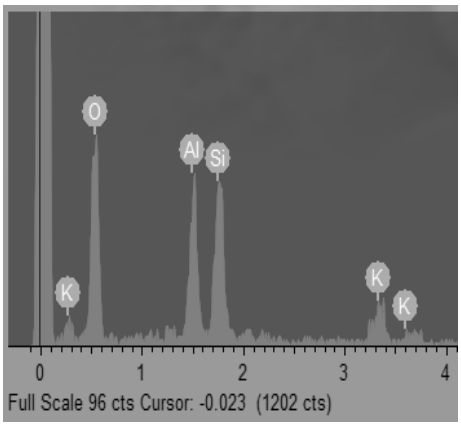

(e)

Figure 5: Scanning electron microscopy and energy dispersive X-ray spectrometry analysis of an agglomerate formed in Run 1 where bed material was bonded together by a black matrix. (a) and (b) present SEM of the surface of the agglomerate; (c) presents SEM of the surface of the porous binding material and (d) presents SEM of the cross section of the porous binding material; (e) presents EDS of the surface of the particle.

Individual grains of bed material which had a glossy appearance were observed in a third category of agglomerates collected from Runs 1 and 2. SEM analysis of such an agglomerate

collected during Run 1 revealed a coating consisting of both rough and smooth areas. Within an identified smooth area, 12,821 times magnification revealed the presence of holes in the relatively homogenous surface. At this level of magnification it was also evident that particles were embedded under the surface of the coating (Figure 6 (c)). EDS analysis identified K, Ca, Mg, and Si in these smooth areas. EDS analysis indicated the presence of K, Ca, Mg, Al, and Si in the rough areas.

SEM analysis of a cross section of a similar agglomerate collected during Run 2 revealed a porous-like structure to the bonds: this arose from numerous chambers contained in the bond. A small number of particles were embedded into the surfaces of these chambers. EDS analysis indicated the presence of K, Ca, Na, Al, and Si in the porous bonds.

In Run 1 an additional type of agglomerate was evident with individual particles encased and bonded together by a glassy, homogenous material (Figure 6 (d)). Initial SEM analysis of the agglomerate showed a coating, the majority of which consisted of a fused and homogenised material, with attached particles scattered across its surface. Increasing to 8,553 times magnification revealed particles embedded in the fused coating (Figure 6 (e)). EDS analysis of the surface of the coating identified the presence of K, Ca, Al, Mg, and Si. An area with contrasting morphology to the majority of the coating consisted of smooth particles fused together. The neck-like bond between these particles showed a porous structure that comprised of K, Ca, and Si (Figure 6 (f)).

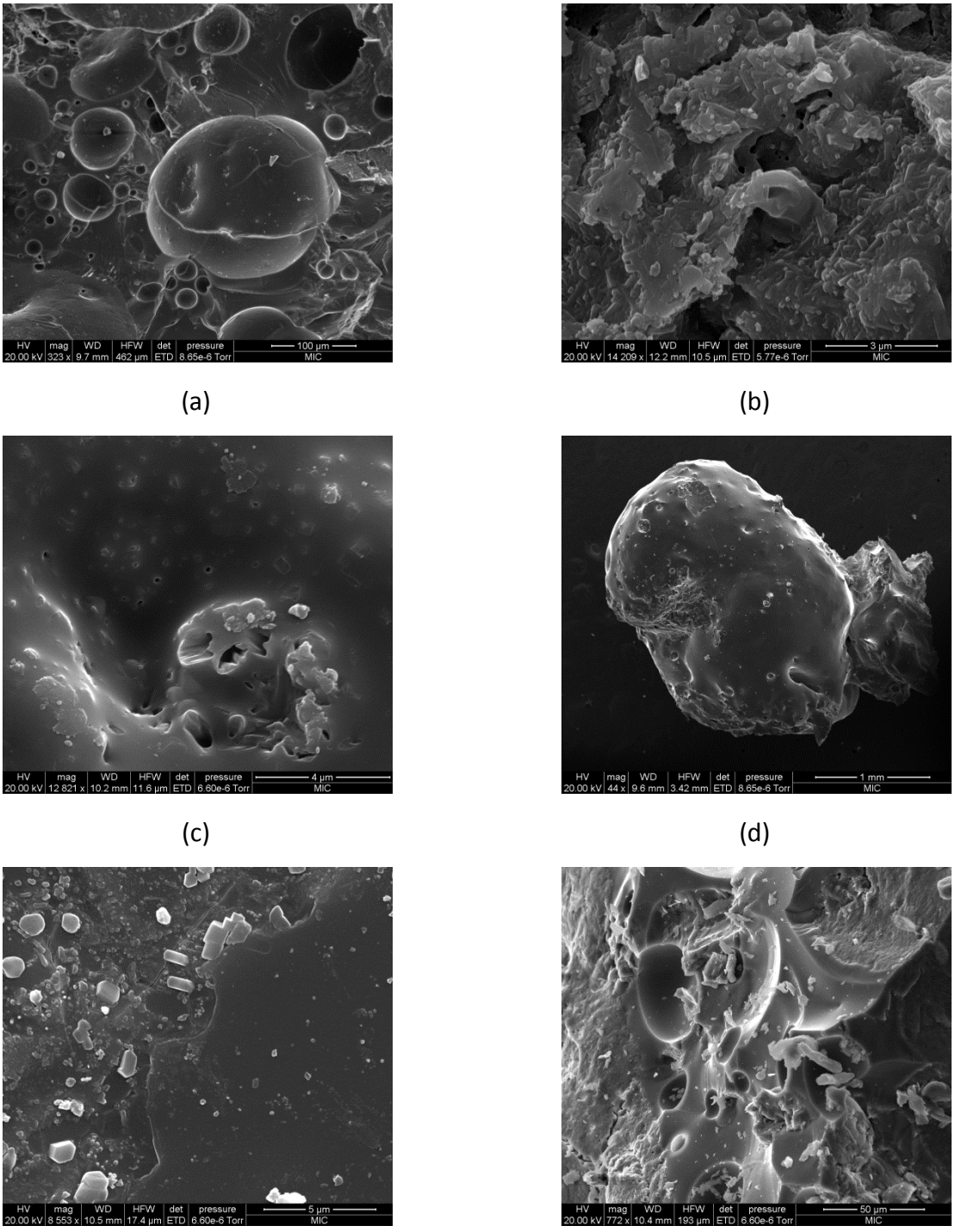

Figure 6: Scanning electron microscopy of agglomerates formed where the bonded bed material had a visible sheen (a through to c) and where a glassy coating was evident (d through to f).

Terracotta-coloured particles were collected from each of the three gasification tests. SEM analysis of the terracotta particles collected from Run 1 revealed a largely smooth surface. EDS analysis indicated the presence of K, Ca, and Si. Particles and holes were scattered

across the surface and small features that were relatively rough were evident. Under high magnification (28,113 times) it was evident that these features consisted of particles fused together (Figure 7 (a)). Larger expanses of rough surface were also evident which showed a transition from the smooth areas, with particles partially embedded into a relatively homogenous fused surface (Figure 7 (b)). Particles were also visible under the coating's surface: K, Al, and Si were identified in these areas by EDS analysis. Under high magnification (31,358 and 96,776 times) globules were apparent on the surface of the fused surface.

SEM analysis of the terracotta particles collected from Run 2 showed an outer surface that had a layered structure with areas of relatively flat layers as well as areas consisting of more granular material. Within the flat layers EDS analysis revealed the presence of K, Ca, Mg, Al, and Si; EDS analysis of the cross section showed the presence of the same elements. Particles were also collected in Run 2 which approached the colour of terracotta but which were considerably darker than the particles collected in Run 1. Through SEM analysis the outer surface was seen to be rough and built progressively of layers of relatively flat material (Figure 7 (c)). Some cracks were observed in the surface of the particle; the fracture mechanism of the particles suggests a laminar structure (Figure 7 (d)). The cross section of the particle showed that it consisted of a relatively smooth material and EDS analysis revealed the presence of Ca and Si.

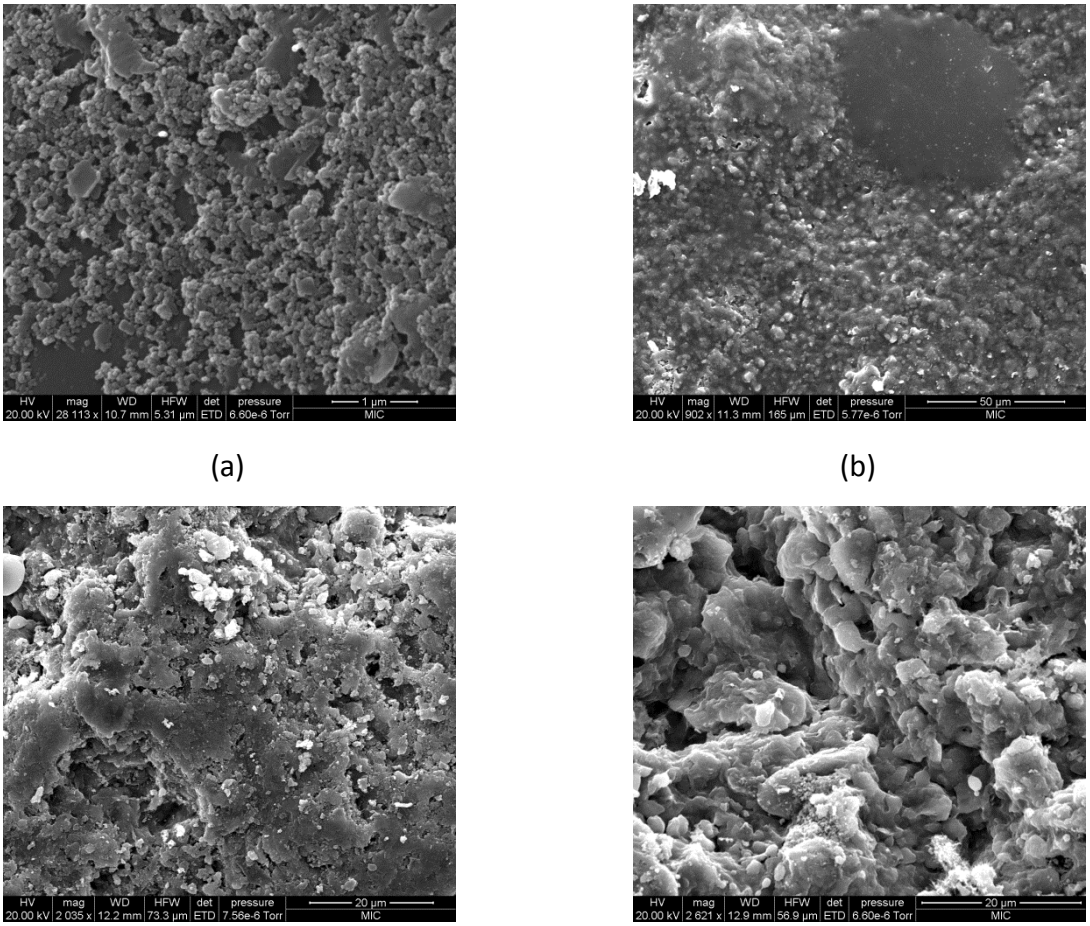

Figure 7: Scanning electron microscopy of agglomerates formed that approached the colour of terracotta. (a) and (b) are in relation to Run 1 while (c) and (d) pertain to Run 2.

It is evident from the EDS analysis of the agglomerates that the material bonding together the bed particles of the alumina sand had a porous structure. This structure was not only present in the relatively thick coatings which, in some instances, fully encased the bed material but was also observed within a neck-like bond connecting two bed particles. The connection of bed material via neck-like bonds is characteristic of viscous sintering or coating-induced agglomeration. The glassy appearance of the bonded particles is in line with the highly viscous melt formed in coating [7] that can remain in a glassy phase at temperatures below its solidus value [6]. Such bonds were observed by Arvelakis et al [8] where a sticky layer containing potassium led to agglomeration. That the agglomerates consisted of only two particles agrees with results reported by Fryda et al [6] who noted agglomerates consisting of two or three particles being produced by coating-induced agglomeration after the gasification of giant reed and sorghum. Fryda et al [6] reported a

porous structure in the case of ash melting, however this was not evident in this experimental work.

The presence of porous structures, though not described by the authors, is evident in SEM analysis presented by Öhman and Nordin [35] and Zevenhoven-Onderwater et al [11]. The porosity in those cases appears much less pronounced than was observed in this study. The porous structure indicates that sufficient time was not available for the bond to homogenise further and reduce its surface energy [7]. Its high porosity also suggests that the bonds are examples of the early stages of agglomerate formation.

Coating-induced agglomeration is associated with the reaction of alkali metals with silica. This is consistent with the results of the EDS analysis of the coating on the bed particles and the neck-like bond between them. Specifically, EDS of the surface of the particle coating revealed the presence of K, Ca, Mg, Al, and Si. In the case of the neck K, Ca, and Si were present. This corresponds with the findings of Zevenhoven-Onderwater et al [11] who reported the main elements of the bridges and coatings of agglomerates as Si, K, and Ca and of Bartels et al. [36] who suggested that K and Na were associated with agglomeration in fluidised beds due to the formation of low-melting silicates.

EDS analysis highlighted the homogenisation of coating layers and the progressive encasement of particles. High magnification revealed this to occur not only in the relatively rough areas of the coating but also in those areas that appear smooth and homogenous at relatively low magnification. This fits with the three step agglomeration model suggested by Öhman and Nordin [35] who postulated that agglomeration was initiated by ash deposition and the homogenisation and strengthening through sintering of the innermost region of this ash coating. In the gasification of various biomass fuels the inner homogenous layer has been identified as consisting primarily of K-Ca-silicates and the outer layer as being particle-rich [35]. All EDS readings performed in this experimental work indicated the presence of K and Si. EDS also highlighted the general presence of Ca in coatings and bonds between particles of agglomerates.

4. Conclusions

The ashing of wheat straw at various temperatures showed a reduction in the quantity of

ash recovered with increasing temperatures (550 - 750 °C), a trend which was also evident in other studies. This illustrates the importance of conducting ashing in a consistent fashion. Ash analysis from this study was used to calculate the Alkali Index, Bed Agglomeration Index, and the Base to Acid Ratio agglomeration indices for wheat straw, and for comparison these indices were also calculated for fuels that were observed to cause agglomeration in other gasification studies. The indices were observed to not predict agglomeration in all cases; indeed, in no case did all indices correctly predict agglomeration. The Alkali Index was found to be the most successful indicator, predicting agglomeration for 7 of the 9 fuels where agglomeration occurred. It also predicted agglomeration for the wheat straw gasified in this study.

During the gasification with air of wheat straw it was observed that the temperatures along the height of the small scale BFB aligned prior to any marked drop in pressure or heating of the lower freeboard, which is characteristic of bed channelling and stratified combustion of biomass above the bed. This convergence was seen to occur in separate gasification experiments at temperatures close to 750 °C. This is low given the use of mullite as bed material, however assessment of other gasification studies indicates that in order to avoid agglomeration at temperatures greater than 800 °C use of alternative bed material alone is insufficient and reactor design must also be considered.

Inspection of the agglomerates formed during the gasification experiments showed that the majority of the agglomerates consisted of individual bed particles bonded together. SEM analysis revealed that the bed particles were connected via neck-like bonds or were embedded either partially or fully into a bonding matrix. SEM analysis of the agglomerates formed identified a porous structure to the material bonding the bed particles together. The extent of the porosity suggests that the bonds are examples of the early stages of agglomerate formation. This structure was not only present in the relatively thick coatings but was also observed within neck-like bonds connecting bed particles. The presence of neck-like bonds indicate viscous sintering or coating-induced agglomeration which is the more commonly reported agglomeration mechanism. Coating-induced agglomeration is associated with the reaction of alkali metals with silica, and EDS analysis indicated the presence of K, Ca, Mg, Al, and Si in the coating of the bed particles and K, Ca, and Si in the

neck-like bonds which is consistent with this method of agglomeration.

Further SEM analysis under higher magnification revealed the coatings of agglomerates to have a layered structure, where ash particles were subsumed into a fused material. This aligns with the three step agglomeration model postulated by Öhman and Nordin [35] where agglomeration commences with ash deposition followed by homogenisation and strengthening through sintering of the innermost region of this ash coating. With EDS analysis indicating the presence of K and Si both on the surface and within the cross section of all agglomerates and the general presence of Ca in coatings and bonds between particles of agglomerates, the results also align with those from other studies highlighting that the inner homogenous layer consists primarily of K-Ca-silicates.

5. Acknowledgements

This study was funded under the Charles Parsons Energy Research Award of Science Foundation Ireland [Grant Number 6C/CP/E001] supported by the Department of Communications, Energy and Natural Resources of the Government of Ireland.

6. References

[1] W. Hongli, M. Yitai and L. Minxia, Research on high efficient straw gasifier, in: D.Y. Goswami and Y. Zhao (Eds), Proceedings of ISES World Congress 2007 (Vol. I – Vol. V), Springer, Berlin, 2009, pp. 2383-2387.

[2] K. Maniatis, Progress in biomass gasification: an overview, in: A.V. Bridgwater (Ed), Progress in Thermochemical Biomass Conversion, Blackwell Science Ltd, Oxford, 2001, pp. 1-31.

[3] E. Natarajan, A. Nordin and A.N. Rao, Overview of combustion and gasification of rice husk in fluidized bed reactors, Biomass Bioenerg. 14 (1998) 533-546.

[4] H. Liu, Y. Feng, S. Wu and D. Liu, The role of ash particles in the bed agglomeration during the fluidized bed combustion of rice straw, Bioresource Tech. 100 (2009) 6505-6513.

[5] E. Natarajan, M. Öhman, M. Gabra, A. Nordin, T. Liliedahl and A.N. Rao, Experimental determination of bed agglomeration tendencies of some common agricultural residues in fluidized bed combustion and gasification, Biomass Bioenerg. 15 (1998) 163-169.

[6] L.E. Fryda, K.D. Panopoulos and E. Kakaras, Agglomeration in fluidised bed gasification of biomass, Powder Technol. 181 (2008) 307-320.

[7] A. van der Drift and A. Olsen, Conversion of Biomass, {Private} Prediction and Solution

Methods for Ash Agglomeration and Related Problems. ECN Energy Research Foundation, Petten, the Netherlands, 1999.

[8] S. Arvelakis, H. Gehrmann, M. Beckmann and E.G. Koukios, Effect of leaching on the ash behavior of olive residue during fluidized bed gasification, Biomass Bioenerg. 22 (2002) 55-69.

[9] P. García-Ibañez, M. Arostegui, A. Cabanillas, J.M. Murillo and P.L. García-Ybarra, Biomass circulating fluidized bed gasification: development of a pilot plant for orujillo gasification, 1st World Conference on Biomass for Energy and Industry, Spain, 2000, pp. 1786-88.

[10] German Institute for Standardisation, Testing of Solid Fuels - Determination of Fusibility of Fuel Ash. German Institute for Standardisation, Berlin, 2007.

[11] M. Zevenhoven-Onderwater, R. Backman, B.J. Skrifvars, M. Hupa, T. Liliendahl, C. Rosén, K. Sjöström, K. Engvall and A. Hallgren, The ash chemistry in fluidised bed gasification of biomass fuels. Part II: Ash behaviour prediction versus bench scale agglomeration tests, Fuel 80 (2001) 1503-1512.

[12] J. Parikh, S.A. Channiwala and G.K. Ghosal, A correlation for calculating HHV from proximate analysis of solid fuels, Fuel 84 (2005) 487-494.

[13] D. Vamvuka, D. Zografos and G. Alevizos, Control methods for mitigating biomass ash-related problems in fluidized beds, Bioresource Tech. 99 (2008) 3534-3544.

[14] T. Kupka, M. Mancini, M. Irmer and R. Weber, Investigation of ash deposit formation during co-firing of coal with sewage sludge, saw-dust and refuse derived fuel, Fuel 87 (2008) 2824-2837.

[15] C.B. Parnell Jr. and W.A. LePori, System and Process for Conversion of Biomass into Usable Energy. US Patent no. 4,848,249, 1988.

[16] S. Capareda and A. Maglinao, Animal manure and other biomass residue conversion into useful energy via fluidized bed gasification, Texas Animal Manure Management Issues Conference, Texas, 2009.

[17] A. Maglinao and S. Capareda, Operation of the TAMU fluidized bed gasifier using different biomass feedstock, ASABE Annual International Meeting, Rhode Island, 2008.

[18] D. Salour, B.M. Jenkins, M. Vafaei and M. Kayhanian, Control of in-bed agglomeration by fuel blending in a pilot scale straw and wood fueled AFBC, Biomass Bioenerg. 4 (1993) 117-133.

[19] A. Ergudenler and A.E. Ghaly, Agglomeration of alumina sand in a fluidized bed straw gasifier at elevated temperatures, Bioresource Tech. 43 (1993) 259-268.

[20] C-E Minerals, MULGRAIN® Grains and Flours, Roswell, Georgia, 2013.

[21] M.J. Fernández Llorente and J.E. Carrasco García, Concentration of elements in woody and herbaceous biomass as a function of the dry ashing temperature, Fuel 85 (2006) 1273-1279.

[22] IEA, Biomass utilization task X, in: Westborg S and N.C. (dk-Teknik) (Eds), Utilization of Straw and Similar Agricultural Residues. Part 1. Recommended Methods for Basic Parameters. Danish Energy Research Project No. 1323/91-0015, vol. 1, International Energy Agency, Paris, 1994, pp. 1-8.

[23] B. Caslin and J. Finnan, Straw for Energy Fact Sheet, in: Tillage no. 12. Teagasc, Oak Park, Carlow, 2010.

[24] B. Olanders and B.-M. Steenari, Characterization of ashes from wood and straw, Biomass Bioenerg. 8 (1995) 105-115.

[25] P. Thy, B.M. Jenkins, S. Grundvig, R. Shiraki and C.E. Lesher, High temperature elemental losses and mineralogical changes in common biomass ashes, Fuel 85 (2006) 783-795.

[26] S.V. Vassilev, D. Baxter, L.K. Andersen and C.G. Vassileva, An overview of the chemical composition of biomass, Fuel 89 (2010) 913-933.

[27] A. Ergudenler and A.E. Ghaly, Agglomeration of silica sand in a fluidized bed gasifier operating on wheat straw, Biomass Bioenerg. 4 (1993) 135-147.

[28] D.L. Carpenter, R.L. Bain, R.E. Davis, A. Dutta, C.J. Feik, K.R. Gaston, W. Jablonski, S.D. Phillips and M.R. Nimlos, Pilot-Scale gasification of corn stover, switchgrass, wheat straw, and wood: 1. Parametric study and comparison with literature, Ind. Eng. Chem. Res. 49 (2010) 1859-1871.

[29] K.D. Panopoulos and D. Vamvuka, Experimental evaluation of thermochemical use of two promising biomass fuels, Proceedings of the European Combustion Meeting 2009, Vienna, 2009.

[30] F. Scala and R. Chirone, An SEM/EDX study of bed agglomerates formed during fluidized bed combustion of three biomass fuels, Biomass Bioenerg. 32 (2008) 252-266.

[31] S.Q. Turn, C.M. Kinoshita and D.M. Ishimura, Removal of inorganic constituents of biomass feedstocks by mechanical dewatering and leaching, Biomass Bioenerg. 12 (1997) 241-252.

[32] C. Hanping, L. Bin, Y. Haiping, Y. Guolai and Z. Shihong, Experimental investigation of biomass gasification in a fluidized bed reactor, Energ. Fuel 22 (2008) 3493-3498.

[33] P. Stoholm, R.G. Nielsen, L. Sarbæk, L. Tobiasen, U.B. Henriksen, M.W. Fock, K. Richardt, B. Sander and L. Wolff, The low temperature CFB gasifier - further test results and possible applications, Proceedings of the 12th European Biomass Conference, Amsterdam, 2002, pp. 706-709.

[34] Energi E2 A/S, Straw Gasification for Co-Combustion in Large CHP Plants: Final Technical Report. Energi E2 A/S and Foster Wheeler Energia Oy, Denmark, 2001.

[35] M. Öhman and A. Nordin, The role of kaolin in prevention of bed agglomeration during fluidized bed combustion of biomass fuels, Energ. Fuel 14 (2000) 737-737.

[36] M. Bartels, W. Lin, J. Nijenhuis, F. Kapteijn and J.R. van Ommen, Agglomeration in fluidized beds at high temperatures: Mechanisms, detection and prevention, Prog. Energ. Combust. 34 (2008) 633-666.